

## Article

# Assessing Soil Organic Carbon Pool for Potential Climate-Change Mitigation in Agricultural Soils—A Case Study Fayoum Depression, Egypt

Mostafa A. Abdellatif <sup>1</sup>, Farag O. Hassan <sup>1</sup>, Heba S. A. Rashed <sup>2</sup>, Ahmed A. El Baroudy <sup>3</sup> ,  
Elsayed Said Mohamed <sup>1</sup> , Dmitry E. Kucher <sup>4</sup> , Sameh Kotb Abd-Elmabod <sup>5</sup> , Mohamed S. Shokr <sup>3,\*</sup>   
and Ahmed S. Abuzaid <sup>2</sup> 

- <sup>1</sup> National Authority for Remote Sensing and Space Sciences, Cairo 11843, Egypt  
<sup>2</sup> Soils and Water Department, Faculty of Agriculture, Benha University, Benha 13518, Egypt  
<sup>3</sup> Soil and Water Department, Faculty of Agriculture, Tanta University, Tanta 31527, Egypt  
<sup>4</sup> Department of Environmental Management, Institute of Environmental Engineering, People's Friendship University of Russia (RUDN University), 6 Miklukho-Maklaya Street, 117198 Moscow, Russia  
<sup>5</sup> Soil and Water Use Department, Agricultural and Biological Research Institute, National Research Centre (NRC), Cairo 12622, Egypt  
\* Correspondence: mohamed\_shokr@agr.tanta.edu.eg



**Citation:** Abdellatif, M.A.; Hassan, F.O.; Rashed, H.S.A.; El Baroudy, A.A.; Mohamed, E.S.; Kucher, D.E.; Abd-Elmabod, S.K.; Shokr, M.S.; Abuzaid, A.S. Assessing Soil Organic Carbon Pool for Potential Climate-Change Mitigation in Agricultural Soils—A Case Study Fayoum Depression, Egypt. *Land* **2023**, *12*, 1755. <https://doi.org/10.3390/land12091755>

Academic Editors: Ioannis Charalampopoulos and Dionisios Gasparatos

Received: 27 July 2023

Revised: 29 August 2023

Accepted: 30 August 2023

Published: 8 September 2023



**Copyright:** © 2023 by the authors. Licensee MDPI, Basel, Switzerland. This article is an open access article distributed under the terms and conditions of the Creative Commons Attribution (CC BY) license (<https://creativecommons.org/licenses/by/4.0/>).

**Abstract:** It is essential to assess the soil organic carbon pool (SOCP) in dry environments to apply appropriate management techniques that address sustainable development. A significant opportunity for sustaining agricultural output and reducing climate change is the storage of soil organic carbon in agricultural soil. The goal of this study was to measure the spatial variability of SOCP content, and determine the effects of soil texture, changes in land use, and land cover on SOCP in surface soil samples. The study additionally investigated the relationships between SOCP and other characteristics, including the normalized vegetation index (NDVI) and land surface temperature (LST), as well as the effects of increasing soil organic carbon on the amount of greenhouse gases. To accomplish this goal, 45 soil surface samples were collected to a depth of 30 cm at the Fayoum depression in Egypt, and analyzed. The soil samples were representative of various soil textures and land uses. The average SOCP concentration in cultivated regions is 32.1 and in bare soils it is 6.5 Mg ha<sup>-1</sup>, with areas of 157,112.94 and 16,073.27 ha, respectively. According to variances in soil textures, sandy soils have the lowest SOCP (1.8 Mg ha<sup>-1</sup>) and clay loam soils have the highest concentrations (49 Mg ha<sup>-1</sup>). Additionally, fruit-growing regions have the greatest SOCP values and may therefore be better suited for carbon sequestration. The overall average SOCP showed 32.12 Mg C ha<sup>-1</sup> for cultivated areas. A rise in arable land was accompanied by a 112,870.09 Mg C rise in SOCP. With an increase in soil organic carbon, stored carbon dioxide emissions (greenhouse gases) would be reduced by 414,233.24 Mg CO<sub>2</sub>. We should consider improving fertilization, irrigation methods, the use of the multiple cropping index, decreasing desertion rates, appropriate crop rotation, and crop variety selection. The research highlights the significance of expanding cultivated areas towards sustainable carbon sequestration and the climate-change-mitigation potential.

**Keywords:** sustainable carbon sequestration; NDVI; land surface temperature (LST); greenhouse gases mitigation; Fayoum depression

## 1. Introduction

Soil organic carbon (SOC) is a crucial component of both food security and climate change mitigation, through carbon sequestration [1]. It is a crucial indicator for determining and controlling soil fertility, soil quality, and soil degradation [2,3]. Changes in land use over the past few decades have had a considerable impact on the global warming process

through carbon dioxide (CO<sub>2</sub>) emissions. However, the reduction in atmospheric CO<sub>2</sub> rates may be aided by carbon sequestration in terrestrial ecosystems [4]. For instance, it has been estimated that croplands can annually store a carbon concentration ranging from 0.90 to 1.85 Pg, which equates to 26% to 53% of the initiative's "4 per 1000" target for soil carbon sequestration [5]. Hence, increasing SOC sequestration through agricultural management approaches has the potential to reduce greenhouse gas emissions by some amount [6]. There is concern that if SOC content in soils reduces too much, the soil physical qualities would degrade and soil nutrient cycling processes will become impaired, which will affect agriculture's ability to produce [7,8]. In terms of particle size distribution and SOC content, soil erosion is a selective process; the eroded material contains more fine soil particles and organic matter than the source material did [9–11]. A positive correlation exists between SOC content and the quantity of 63 µm sized fine-grained particles [9]. Additionally, it was discovered that 77% of the SOC in cultivated soils is preserved in the proportion of particles of 20 µm and that 86% to 91% of the SOC is connected with soil mineral particles [12,13]. According to data from the World Bank in 2016, agricultural land covers around 38.18% of the global area and is the main land-use type among all land-use types [14]. Egypt's land area (96%) is classed as desert and has a very-high-to-high sensitivity to desertification. Over the past 35 years, successful attempts to reclaim desert regions have been made by the public and private sectors, totaling more than one million feddans (feddan = 0.42 hectare) [15].

The change in SOC storage is constantly influenced by agricultural activity and production [16,17]. Therefore, it is important to look at the SOC's geographical and temporal distribution patterns in agricultural regions. SOC, the primary soil fertilizer, has an impact on soil composition and crop growth [18]. The type and quantity of carbon that enters the soil system, as well as the physical makeup of the root zone, have the most effects on plants. This has indirect impacts on the biomass and composition of the microbial community [19]. Moreover, plant biomass production is enhanced by carbon resources [20]. Additionally, the climate may change the activity of soil microbes, which could affect SOC humification and modify its chemical composition [21,22].

The normalized difference vegetation index (NDVI) is a crucial indicator of crop biomass and growth use [14]. Many factors, including soil type, soil management techniques, and climate conditions, affect the soil's capacity to store organic matter [23–25]. Although the temperature harms SOC vertical distribution, precipitation has a favorable impact on SOC content [26]. One of the world's most environmentally vulnerable areas is Egypt, a country that is primarily desert and hyperarid. In the context of global warming, the nation became a hotspot for climatic extremes and aridity change [27]. Research on land surface temperature (LST) variations is more crucial in arid areas [28]. Trends and variability in surface temperature are found using satellite images as a source of data [29]. The capacity to measure earth's surface conditions, the availability of high resolution, and consistent and repeating coverage are all benefits of utilizing remotely sensed data [30]. Low atmospheric precipitation is one of the most noticeable characteristics of arid regions which directly impacts the soil moisture content and indirectly influences the vegetation conditions in these locations [31]. Thus, in drylands, there is a greater need for attention given to the effects of climate change and potential food security adjustments [32]. Understanding the current level and spatial distribution of SOC can aid in quantifying and tracking carbon, which can aid in increasing the amount of carbon sequestered in soils to reduce concerns about climate change [33].

Many studies have demonstrated the strong spatial dependency of soil properties, and soil mapping has effectively employed trend soil-surface analysis, inverse-distance-weighted models, and geostatistical models [34–36]. Kriging is an effective geostatistical method for examining the geographical distribution of soil properties and incorporating data into raster maps through spatial interpolation [37,38].

The study hypothesizes that many factors, including soil texture, land use, and LST, may have an impact on some characteristics, such as carbon sequestration ability, and as a

result, have an impact on CO<sub>2</sub> mitigation. Thus, the objectives of the current study were to: (1) assess and demonstrate spatial variability of SOCP content; (2) ascertain the effects of soil texture and changes in land use and land cover on SOCP in the surface soil samples; (3) examine the relationships between SOCP and other attributes such as NDVI and LST; and (4) evaluate the effects of an increase in soil organic carbon on the amount of greenhouse gases (GHGs) in the atmosphere as a result of carbon dioxide emissions.

## 2. Methodology

### 2.1. Investigated Region

The Fayoum depression in Egypt's Western Desert occupies an area of roughly 2302.67 km<sup>2</sup> (230,267 hectares) (total study area). Its boundaries are 29°10' and 29°34' E longitude and 30°15' and 31°06' N latitude (Figure 1). According to the research area's climate data, the mean minimum and highest annual temperatures are 14.5 and 31.0 °C, respectively, and the mean annual precipitation is 7.2 mm. The highest daily evapotranspiration rate was 7.3 mm, while the lowest rate was 1.9 mm, which occurred in January. The soil's temperature and moisture levels are governed by thermal and torric regimes, respectively [39]. The canal of Hawara, which carries water to the depression, connects it to the Nile River [40]. Lacustrine plain, fluvial-lacustrine plain, and alluvial plain are the three main landscapes that make up the physiographic units of the El-Fayoum depression [41,42]. The study area is distinguished by an elevation that reaches 23 m above sea level [43]. Six districts comprise the research area (Tamia, Sinnoris, Ibshawai, Fayoum, Yousef El Sadik, and Itsa). In the research area, agriculture dominates [44].

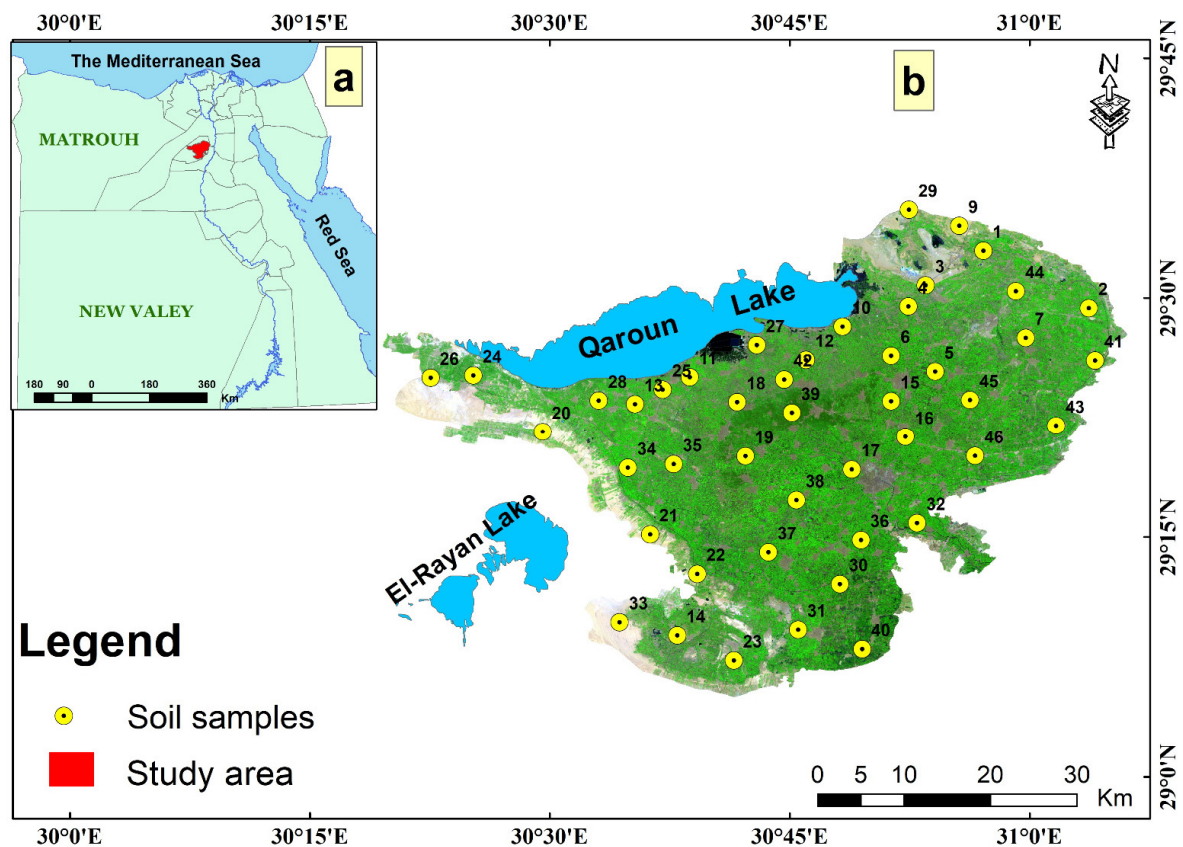


**Figure 1.** Research area's location (a) map of Egypt, (b) Fayoum depression (study area).

### 2.2. Soil Samples and Laboratory Analysis

Forty-five soil surface samples were collected to a depth of 30 cm (Figure 1). Utilizing GPS, the coordinates of each location were recorded. In each location, a single mixed sample (from three replicates) that characterized the root-zone soil was taken. The chosen

locations illustrate the spatial changes that have occurred in the research area, which is defined by a wide range of physiographic characteristics [42]. The samples were air-dried, crushed, and put through a 2 mm sieve to prepare them for physical and chemical examinations. A glass electrode was used to test the soil reaction (pH) of a 1:2.5 soil-to-water solution [34] using the pH meter Europe/Romania, model/type HI2211 HANNA. In saturated soil paste extract, the electrical conductivity (ECe) of the soil was measured [45] using an EC meter EUTECH-Singapore, model/type CON 2700. The instrument was calibrated using standard pH and conductivity solutions prior to the analyses. Based on the mathematical formula provided by [35], the exchangeable sodium percentage (ESP) was calculated ( $ESP = \text{exchangeable} \frac{Na}{CEC} \times 100$ ). Cation-exchange capacity (CEC) was measured using the sodium acetate technique [46]. The calcium carbonate ( $CaCO_3$ ) was analyzed by applying hydrochloric acid (HCL) to 1 g of dry soil and gypsum, based on guidelines of [47]. The soil organic matter (SOM) was measured via titration and acid-dichromate potassium (the Walkley and Black procedure) [46,48]. Using the international texture triangle and the international pipette method, soil particle studies were carried out relying on the percentage of sand, silt, and clay in the soil. When analyzing soil texture using the pipette method, the soil is first mechanically and chemically dispersed, and then it is fractionated. Sedimentation is then used to determine the silt and clay fractions after quantifying the sand fraction through sieving [49]. Using soil core samples, bulk density (BD) was measured [50]. The cores' contents were weighed after drying for 24 h at 105 °C in an oven. The dry weight-to-volume ratio provides the BD [51].

### 2.3. Statistical Analysis

Using SPSS version 25, the minimum, maximum, arithmetic mean, standard deviation, skewness and kurtosis of the investigated soil properties were calculated. The Pearson correlation coefficient was utilized to show linear relationships between studied variables.

### 2.4. Geostatistical Analyses

The simple Kriging interpolation method was used to create maps showing the spatial distribution of soil parameter patterns [42,52]. With ArcGIS software 10.4, the geostatistical studies use the Kriging interpolation method [53]. The best model that matched for the chosen soil parameters was determined in the current study using semi-variogram models (Gaussian, circular, and spherical). According to [54], the accuracy of the various models has been assessed based on the mean standardized error (MSE), and root-mean-square error (RMSE) Equations (1)–(3). The correctness of the model was shown by the values of MSE and root-mean-square standardized error (RMSSE) that were closest to zero and one, respectively [55–58].

$$MSE = \frac{1}{n} \sum_{i=1}^n [x_i - y_i] \quad (1)$$

$$RMSE = \sqrt{\frac{1}{n} \sum_{i=1}^n [x_i - y_i]^2} \quad (2)$$

$$RMSE = \sqrt{\frac{1}{n} \sum_{i=1}^n [x_i - y_i]^2 / \sigma M(y_i)} \quad (3)$$

where  $x_i$  and  $y_i$  represent the measured and expected values, respectively,  $n$  denotes the quantity of predicted values among a set of nearby soil samples, and  $\sigma M$  the standardized error of predicted values.

### 2.5. Remote Sensing and Image Analysis

#### 2.5.1. Supervised Classification

For the supervised image categorization of the research area, the Landsat 7 ETM+, which captured data on 27 June 2000, and the Operational Land Imager (OLI), which captured data on 26 August 2013 and 20 August 2022, with a spatial resolution of 30 m, were

employed. The image preprocessing based on radiometric and atmospheric calibrations were carried out using ENVI software version 5.3. A supervised maximum likelihood classification was utilized to categorize the satellite image to produce land-use maps [59].

### 2.5.2. Image Analysis for Land Surface Temperature (LST)

ArcGIS 10.4 was used to construct the algorithm. In this work, brightness temperatures were estimated using bands 10 and 11 of Landsat 8's thermal infrared data, while the NDVI was computed using bands 4 and 5. The USGS website for extracting top-of-atmosphere (TOA) spectral radiation is where the LST retrieval formulae were obtained from [60].

### 2.5.3. The Conversion of Digital Numbers (DN) to the Top-of-Atmosphere Radiance (TOA)

Using the radiance rescaling factors provided in the metadata file, the thermal band data DN were transformed to TOA spectral radiance [61] according to Equation (4).

$$L_{\lambda} = M_l \times Q_{cal} + A_l \quad (4)$$

where:

$L_{\lambda}$  = the TOA's spectral radiance in watts/(m<sup>2</sup>\*srad\*m),

$M_l$  = a band-specific multiplicative rescaling factor from the metadata (RADIANCE MULT BAND x),

$Q_{cal}$  = a set of quantized and calibrated standard-product pixel values (DN),

$A_l$  = a band-specific additive rescaling factor from the metadata (RADIANCE ADD BAND x).

### 2.5.4. Transforming TOA into At-Satellite Brightness Temperature

Using Equation (5), the thermal constants in the MTL file can be used to transform thermal band data from spectral radiance to top-of-atmosphere brightness temperature [61].

$$BT = K_2 \div \ln \left[ \left( \frac{K_1}{L_{\lambda}} \right) + 1 \right] - 273.15 \quad (5)$$

where:  $BT$  = top-of-atmosphere brightness temperature (°C),  $K_1 = K_1$  constant band (No.), and  $K_2 = K_2$  constant band (no.).

### 2.5.5. Normalized Difference Vegetation Index (NDVI) Calculation

A close relationship exists between drought conditions and the normalized difference vegetation index (NDVI), which is obtained from remote-sensing (satellite) data. The varied colors (wavelengths) of visible and near-infrared sunlight reflected by the plants are examined to identify the density of green on a piece of land; red and near-infrared bands, i.e., Bands 4 and 5 (Landsat OLI 8), and Bands 3 and 4 (Landsat 7 ETM+), were utilized for the normal NDVI calculation, respectively. Since NDVI can be used to estimate general vegetation status and since the amount of vegetation present is a significant influence, estimating the NDVI is crucial. The NDVI calculation based on Equations (6) and (7) is crucial because it should be followed by calculations of the proportion of vegetation (PV), which are closely related to the NDVI, and emissivity ( $\epsilon$ ), which is related to both. The values of NDVI in the year 2022 were used in the calculation of LST. The NDVI for Landsat OLI 8 is calculated using the following equation.

$$NDVI = \frac{Band\ 5 - Band\ 4}{Band\ 5 + Band\ 4} \quad (6)$$

This equation expresses the calculation of NDVI for Landsat OLI 8, where *Band 4* stands for the red band (wavelength = 0.64–0.67  $\mu$ m), and *Band 5* for the near-infrared band (NIR) (wavelength = 0.85–0.88  $\mu$ m).

The calculation of NDVI for Landsat 7 ETM+ is expressed by the following

$$NDVI = \frac{Band\ 4 - Band\ 3}{Band\ 4 + Band\ 3} \quad (7)$$

where *Band 3* stands for the red band (wavelength = 0.63–0.69  $\mu\text{m}$ ), and *Band 4* for the near-infrared band (NIR) (wavelength = 0.77–0.90  $\mu\text{m}$ ).

#### 2.5.6. Determining the Vegetation Proportion

The percentage of ground covered by vegetation in a vertical projection is referred to as the vegetation fraction (proportion of vegetation). Via plant transpiration, surface albedo, emissivity, and roughness, changes in vegetation cover have a direct impact on surface water and energy budgets [62]. The NDVI readings for soil and vegetation are strongly connected to the percentage of vegetation ( $P_v$ ). The standard NDVI approach was used to estimate ( $P_v$ ) in this study, as shown in Equation (8) [63].

$$P_v = \left[ \frac{NDVI - NDVI_{Min}}{NDVI_{max} + NDVI_{Min}} \right]^2 \quad (8)$$

where  $NDVI_{Min}$  and  $NDVI_{max}$  = the minimum and maximum values of the NDVI, which stand for the NDVI of the vegetation and the soil, respectively.

#### 2.5.7. Land Surface Emissivity ( $\epsilon$ ) Calculation

The land surface emissivity ( $\epsilon$ ), calculated from the measured radiance and land surface temperature, which is the average emissivity of a surface element on Earth, is based on Equation (9). In cases where the NDVI is less than 0, water is assumed to be present, and an emissivity value of 0.991 is assigned. The emissivity value of 0.996 is given for NDVI values between 0 and 0.2, which indicate that the ground is covered in soil. The emissivity is calculated using [64] and values between 0.2 and 0.5 are regarded as combinations of soil and vegetation cover. In the final scenario, a value of 0.973 is assigned, since vegetation is thought to be present when the NDVI value is larger than 0.5. The emissivity value of 0.986 was ascribed to this study, however, because the typical NDVI value lies from less than 0 to more than 0.5.

$$\epsilon = 0.004 \times P_v + 0.986 \quad (9)$$

where:  $\epsilon$  is Land Surface Emissivity, and 0.986 is the blackbody radiance factor according to Planck's law.

#### 2.5.8. Calculating Land Surface Temperature (LST)

As shown in Equation (10) below, the emissivity-corrected land surface temperature (LST) is calculated.

$$LST = \frac{BT}{1 + (11.5 (BT) \times \ln(\epsilon/1.483 \times 10^{-2}))} \quad (10)$$

where  $LST$  is expressed in degrees Celsius,  $BT$  is the temperature of the at-sensor brightness in Celsius,  $\lambda$  ( $\mu\text{m}$ ) is the wavelength of the emitted radiation:  $\rho$  (mK). The Stefan–Boltzmann constant is equal to  $\sigma$ . Planck's constant is equal to  $h$ , light velocity is equal to  $c$ , and emissivity of the land surface is equal to ( $\epsilon$ ).

#### 2.6. Calculation of the Soil Organic Carbon Pool (SOCP)

The relationship between SOCP and soil organic carbon (SOC) concentration was examined [1]. Data for soil organic matter content were first multiplied by a factor of 0.58 to obtain SOC % [65]. The soil organic content percentage (SOC) was multiplied by the soil bulk density ( $\text{Mg m}^{-3}$ ) within the sampled soil depth (cm) and the fine soil fraction (2 mm

in size) to determine the mass-per-unit area ( $\text{kg m}^{-2}$ ) for each soil profile at the top 30 cm depth [65], as shown in Equation (11).

$$SOCP = [L \times SOC \times B.D \times (1 - \frac{F}{100})]/10 \quad (11)$$

where *SOCP* is the soil organic carbon pool surface-soil samples (30 cm), *L* is the soil layer thickness, (cm), *SOC* is the soil organic carbon, B.D. is the dry bulk density of the soil, ( $\text{Mg m}^{-3}$ ), and *F* is the coarse soil fragment of more than 2 mm (wt.%).

### 2.7. Mitigation of Carbon Dioxide ( $\text{CO}_2$ )

The following Equation (12) was used to determine the mitigation emitted carbon dioxide ( $\text{CO}_2$ ), based on the soil organic carbon sequestered in the soil surface. The molecular weight of  $\text{CO}_2$  divided by the atomic weight of carbon results in a factor of 3.67. The weighted average of molecules carrying the various carbon isotopes found in the atmosphere, primarily  $^{12}\text{C}$  and  $^{13}\text{C}$ , was used by Intergovernmental Panel on Climate Change [66] instead of 44 and 12, respectively.

$$\text{MEC} = \text{ASCS} \times 3.67 \quad (12)$$

where MEC = mitigation emitted  $\text{CO}_2$  and ASCS = amount of soil carbon sequestration.

## 3. Results and Discussion

### 3.1. Soil Characteristics within Research Area

Table 1 contains a list of the study area's soil characteristics. The pH values in particular vary from 7.21 to 8.37, with an average value of  $7.84 \pm 0.47$ , indicating that the research region has mildly/strongly alkaline conditions [48]. Higher soil pH causes an increase in the mineralizable portions of N and C ratios, where the linkages between clays and organic components are disrupted [67]. The findings show that the research area has moderate-to-highly salinized soils, with average ECe values of  $4.99 \pm 3.96 \text{ dS m}^{-1}$ , and ranges from 1.20 to  $17.40 \text{ dS m}^{-1}$  [68]. High-quality water is required for the leaching of highly salinized soils [69]. The average ESP value is  $15.48 \pm 7.10$ , and the values range from 6.28 to 36.83. This high sodium content might harm soil features like soil structure and hydrology, which will ultimately lower crop yield [42]. The CEC of the research region ranges widely, from 6.35 to  $41.70 \text{ cmol}_c \text{ kg}^{-1}$  soil, with an average of  $22.27 \pm 8.79 \text{ cmol}_c \text{ kg}^{-1}$  soil. Basic alkali cation adsorption and CEC are correlated with clay concentration. The opposite effects that clay and silt have on other soil characteristics depend primarily on their contribution to the soil particle-size distribution, since clay has a higher surface area and CEC than silt [70]. The  $\text{CaCO}_3$  concentrations range from 35 to  $230.9 \text{ g kg}^{-1}$ . The greatest  $\text{CaCO}_3$  values, possibly caused by shell particles, were found in areas near Qaroun Lake, in agreement with [42]. The addition of P fertiliser to calcareous soils with the highest  $\text{CaCO}_3$  values can fix P fertiliser and create very hard layers that are impervious to water and crop roots [71]. The research area has a comparatively low SOM content in line with [42], ranging from 0.7 to  $19.5 \text{ g kg}^{-1}$ , with an average of  $11.1 \pm 5.7 \text{ g kg}^{-1}$ . The SOM is crucial for preserving appropriate soil structure, improving the availability of minerals that enhance soil fertility, and preserving the farm ecosystems [72]. According to the physical characteristics of the research area's soil, sandy clay loam, clay loam, and clay are the most prevalent soil textures; the average dry bulk density was  $1.45 \pm 0.09 \text{ Mg m}^{-3}$ , and ranged from 1.24 to  $1.57 \text{ Mg m}^{-3}$ . The evaluated soil parameters' low skewness and kurtosis values indicated that the distribution was roughly normal.

**Table 1.** Quantifiable information about the variables under investigation.

Characteristics	Statistical					
	Min.	Max.	Mean	Std.	Skewness	Kurtosis
pH	7.21	8.37	7.84	0.22	0.42	1.49
EC (dS m <sup>-1</sup> )	1.20	17.40	4.99	3.96	1.77	2.38
ESP	6.28	36.83	15.48	7.10	1.35	1.54
CEC (cmol <sub>c</sub> Kg <sup>-1</sup> )	6.35	41.70	22.27	9.44	-0.03	-0.75
CaCO <sub>3</sub> (g kg <sup>-1</sup> )	35	230.9	99.9	55.93	1.01	-0.08
Gypsum %	0.11	0.45	0.19	0.08	1.13	1.07
SOM (g kg <sup>-1</sup> )	0.7	19.5	11.11	5.7	-0.54	-1.03
B.D. (Mg m <sup>-3</sup> )	1.24	1.57	1.45	0.09	-0.92	0.41

Min. is minimum, Max. is maximum, Std. is standard deviation, and Mg. is megagram.

### 3.2. Mapping Based on Geostatistical Analysis

Table 2 shows the semi-variogram modeling's parameters. With the use of RMSE, MSE, and RMSSE, the accuracy parameter of the semi-variograms' best-fit model was determined. According to the findings, the Gaussian model was well suited for EC, ESP, CaCO<sub>3</sub>, and gypsum, and the spherical model was suitable for pH, SOM, SOC and BD. The circular model was also well suited for CEC. While the RMSSE values were close to one, the MSE values were nearly zero for all of the parameters that were chosen. The higher portions of the northwest and northeast of the research area, respectively, showed an increase in the spatial patterns of pH and EC (Figure 2) The northeast region, where Qaroun Lake is located, had the highest CaCO<sub>3</sub> levels. The highest values of SOM were found in the middle areas of the study area. The greatest BD values were scattered in several regions to the east and west of the research area, with no obvious spatial pattern (Figure 2).

**Table 2.** Modelling of spatial-data semi-variogram parameters.

Soil Parameters	Model Type	Mean	RMSE	MSE	RMSSE
pH	Spherical	-0.001	0.167	-0.01	0.982
EC	Gaussian	-0.35	3.80	-0.08	1.07
ESP	Gaussian	0.59	8.29	0.08	1.10
CEC	Circular	-0.2738	10.87	-0.02	0.99
CaCO <sub>3</sub>	Gaussian	-0.14	5.47	-0.02	1.00
Gypsum	Gaussian	-0.00	0.07	-0.004	1.03
SOM	Spherical	-0.010	0.651	-0.02	0.99
SOC	Spherical	0.447	12.27	0.030	0.98
BD	Spherical	-0.00	0.082	-0.05	1.02

### 3.3. Interaction between Different Studied Variables

A substantial inverse relationship ( $r = -0.713$ ) between clay and land surface temperature is evident (Table 3), and these outcomes are consistent with Wang et al. 2015 [73]. There is a substantial positive association between soil organic matter, CEC, and clay, and these outcomes are consistent with those in [43]. Bulk density is inversely related to the amount of organic matter in the soil ( $r = -0.55$ ). The bulk density will decrease as the level of organic matter increases [74]. There is a direct correlation between sand percentage and density values, according to the results of the study on the relationship of soil bulk density with texture, total organic-matter content, and porosity; thus, an increase in the amount of organic matter can result in a decrease in the value of density, which is necessary for the proper growth of plants [75]. High soil-density values cause the porosity to decline, which in turn lowers the soil's ability to hold onto water, which is essential for plants to grow properly [76]. The characteristic that needs to be calculated with the highest importance is clay content (soil fraction < 2  $\mu\text{m}$ ), because clays provide some protection against the

oxidation of organic matter, and organic carbon levels rise as clay content increases [77]. This has to do with the ability of soils to exchange cations, and it permits precise control of soil hydraulic characteristics such as water storage and availability to crop plants, field capacity, and wilting point. It is the initial statistical consideration made when developing pedotransfer functions [78–80]. Thus, NDVI and soil clay have a correlation coefficient of ( $r = 0.60$ ). According to [81], NDVI is a highly accurate predictor of SOC levels, which represent the biomass and productivity of vegetation. These results show that NDVI and SOCP have a significant association ( $r = 0.67$ ). There is a significantly inverse ( $r = 0.68$ ) correlation between the NDVI and LST (Table 3). According to Kumar et al., [82], anthropogenic heat release from energy use and a decline in plant cover are both contributing factors to the rise in LST. In the current global climate, increased urbanization, development, and deforestation, which raise LST, have led to a reduction in NDVI [83].

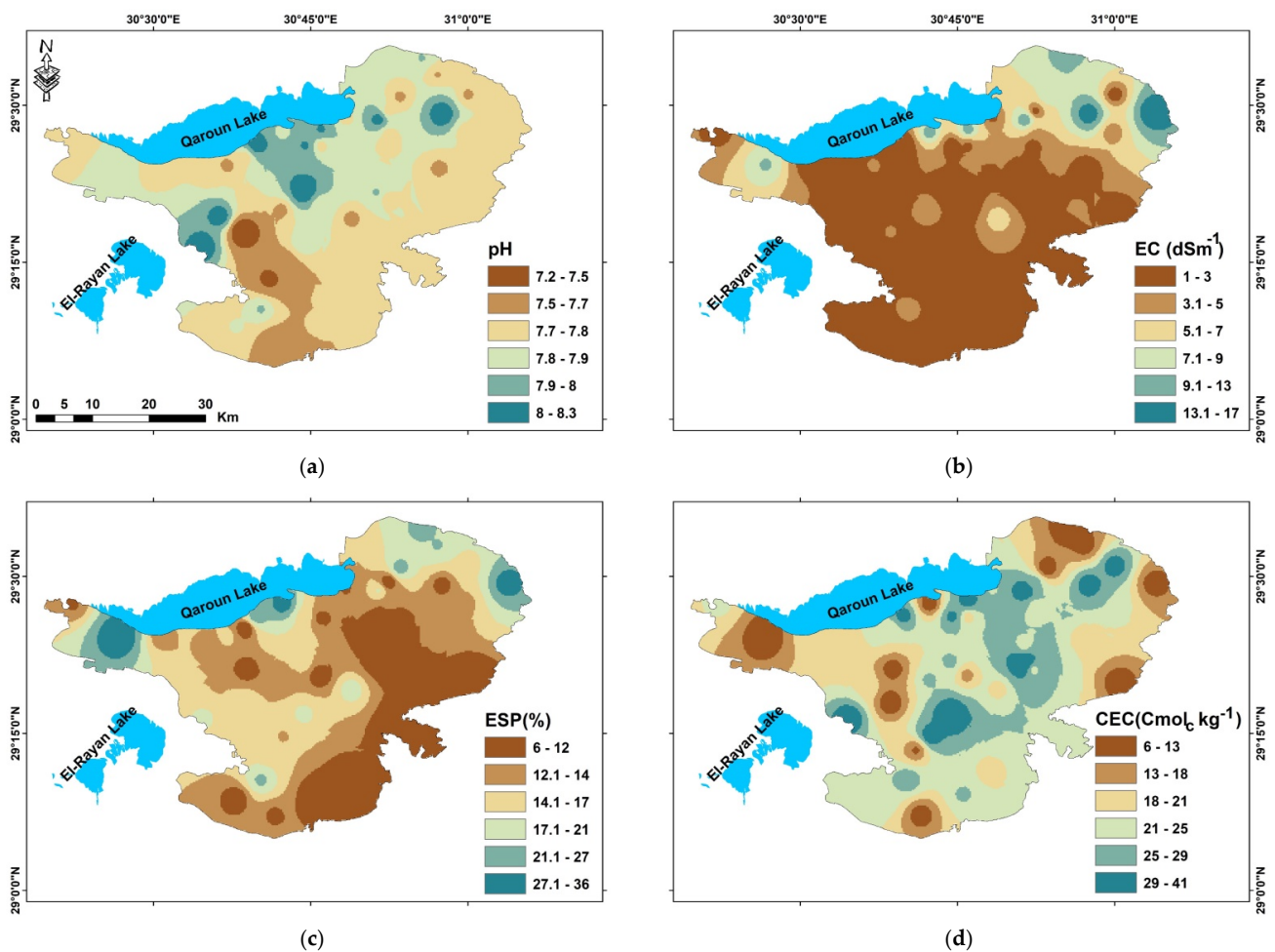
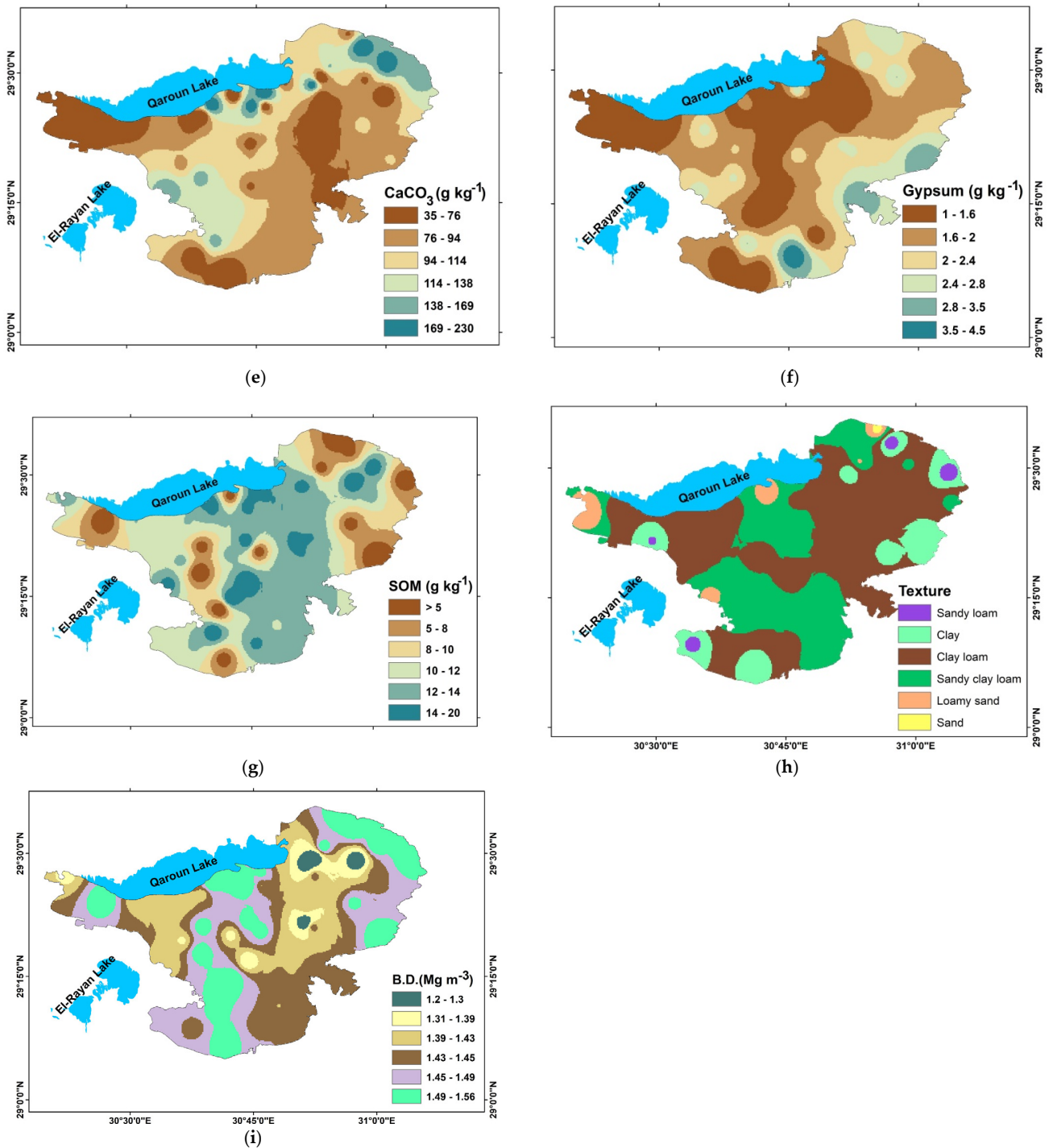


Figure 2. Cont.



**Figure 2.** Interpolation maps of studied variables: (a) soil reaction (pH), (b) electric conductivity (EC: dS/m), (c) exchangeable sodium percent (ESP), (d) cation-exchange capacity (CEC: cmole/kg), (e) calcium carbonate ( $\text{CaCO}_3$ :  $\text{g kg}^{-1}$ ), (f) gypsum ( $\text{g kg}^{-1}$ ), (g) soil organic carbon (SOM:  $\text{g kg}^{-1}$ ), (h) soil texture, and (i) bulk density (B.D.:  $\text{Mg m}^{-3}$ ).

**Table 3.** The analyzed variables' Pearson correlation matrix.

	Clay	CaCO <sub>3</sub>	Gypsum	OM	B.D.	SOCP	CEC	ESP	pH	EC	LST	NDVI
Clay	1	−0.131	−0.124	0.857 **	−0.744 **	0.817 **	0.869 **	−0.522 **	0.268	−0.418 **	−0.713 **	0.606 **
CaCO <sub>3</sub>	−0.131	1	0.205	0.099	0.333 *	0.145	0.181	0.332 *	0.192	0.194	−0.117	0.255
Gypsum	−0.124	0.205	1	−0.057	0.096	−0.061	−0.052	−0.051	0.046	0.146	0.070	−0.082
OM	0.857 **	0.099	−0.057	1	−0.549 **	0.991 **	0.937 **	−0.274	0.510 **	−0.229	−0.806 **	0.689 **
B.D.	−0.744 **	0.333 *	0.096	−0.549 **	1	−0.435 **	−0.586 **	0.408 **	−0.272	−0.009	0.448 **	−0.450 **
SOCP	0.817 **	0.145	−0.061	0.991 **	−0.435 **	1	0.911 **	−0.245	0.493 **	−0.267	−0.803 **	0.676 **
CEC	0.869 **	0.181	−0.052	0.937 **	−0.586 **	0.911 **	1	−0.297 *	0.494 **	−0.221	−0.723 **	0.641 **
ESP	−0.522 **	0.332 *	−0.051	−0.274	0.408 **	−0.245	−0.297 *	1	0.130	0.538 **	0.161	−0.165
pH	0.268	0.192	0.046	0.510 **	−0.272	0.493 **	0.494 **	0.130	1	0.169	−0.0420 **	0.517 **
EC	−0.418 **	0.194	0.146	−0.229	−0.009	−0.267	−0.221	0.538 **	0.169	1	0.078	0.036
LST	−0.713 **	−0.117	0.070	−0.806 **	0.448 **	−0.803 **	−0.723 **	0.161	−0.420 **	0.078	1	−0.793 **
NDVI	0.606 **	0.255	−0.082	0.689 **	−0.450 **	0.676 **	0.641 **	−0.165	0.517 **	0.036	−0.793 **	1

\*\* Correlation is significant at the 0.01 level (2-tailed). \* Correlation is significant at the 0.05 level (2-tailed).

### 3.4. Land-Use Change Detection

The current land use of the research area is depicted in Figure 3. Cultivated areas, barren soils, urban areas, and water bodies were the four classes that were observed. Agriculture areas are the dominant classes, accounting for approximately 157,112.94 ha (68.24%) of the total area. Wheat, sesame, cotton, maize, clover, and several medicinal and aromatic plants are the major field crops in the study area. Fruit trees include mango, guava, grape, citrus, date palm, and olive trees. Urban (residential and industrial areas) are the second dominant class, representing approximately 22,534 ha (9.78%) of the total studied area, while bare soils account for 16,073.27 ha (6.98%) and water bodies account for 34,546 ha (15%). Figure 3 and Table 4 below display how land use in the study area changed between 2000, 2013 and 2022. The change-detection analysis is a useful tool for describing changes seen across all land-use categories. The area of bare soils decreased by an average of 13,507.13 hectares between 2000 and 2022 as a result of land reclamation [84]. Soil salinity and alkalinity were the key factors limiting soil capacity in the study area. The use of tile drainage, low-salt irrigation water, and soil amendment using gypsum or organic matter to improve soil fertility and reduce soil salinity was suggested [42,85,86]. In 2013, particularly, the area of agricultural land was practically steady or had slightly increased, despite the growth of reclaimed land, and this is due to the increase in urbanization. The water bodies decreased by around 1346 ha. The Normalized Difference Vegetation Index (NDVI) correlates soil organic matter and vegetation cover in a direct and indirect manner, respectively [87]. Thus, an increase in cultivated areas of 3513.93 ha caused an increase in NDVI in 2022 (Figure 4). The highest NDVI value recorded in 2000 was 0.67, followed by 0.58 in 2013 and 0.75 in 2022.

**Table 4.** Changes in land use in the Fayoum depression region between 2000, 2013 and 2022.

	Area (ha)			
	2000	2013	2022	Change (2000–2022)
Cultivated areas	153,599	156,133.56	157,112.94	3513.93
Urban area	12,772.7	20,333.75	22,534.79	9762.09
Bare soils	29,580.4	17,907.69	16,073.27	−13,507.13
Water bodies	34,315	35,892	34,546	−231

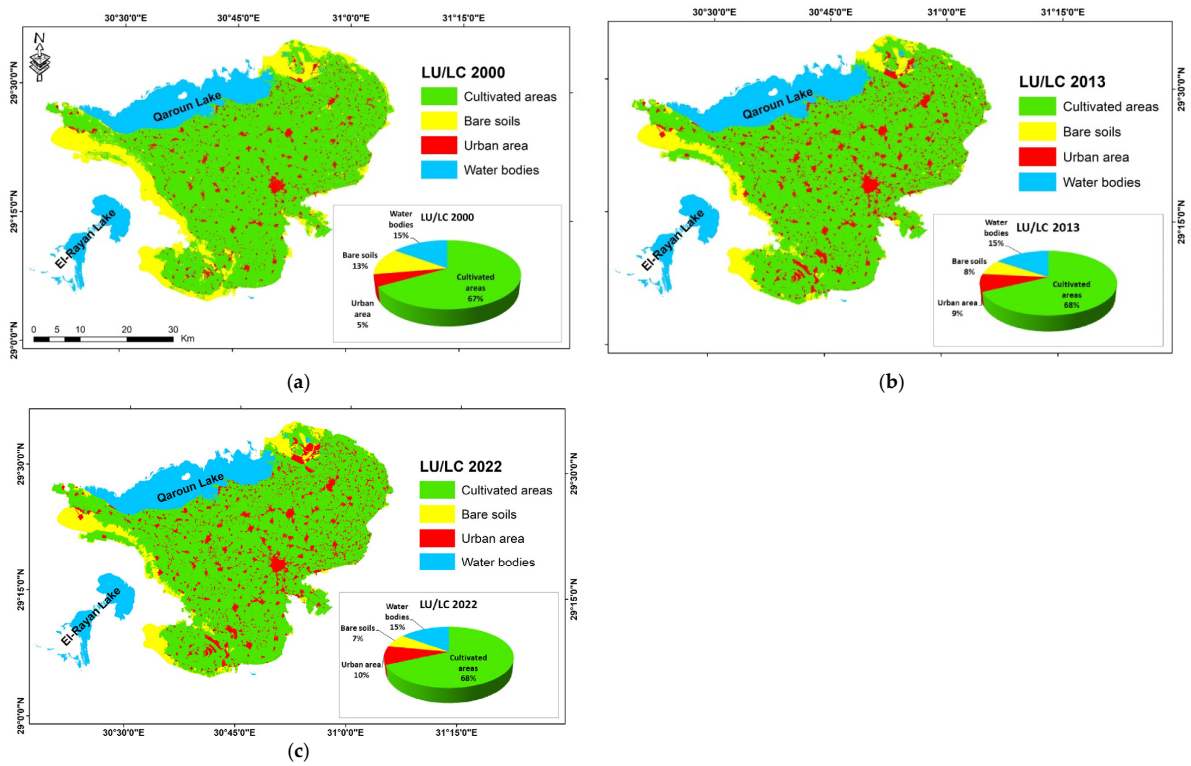


Figure 3. Land Use and Land Cover (LULC) of the study (a) 2000, (b) 2013, and (c) 2022.

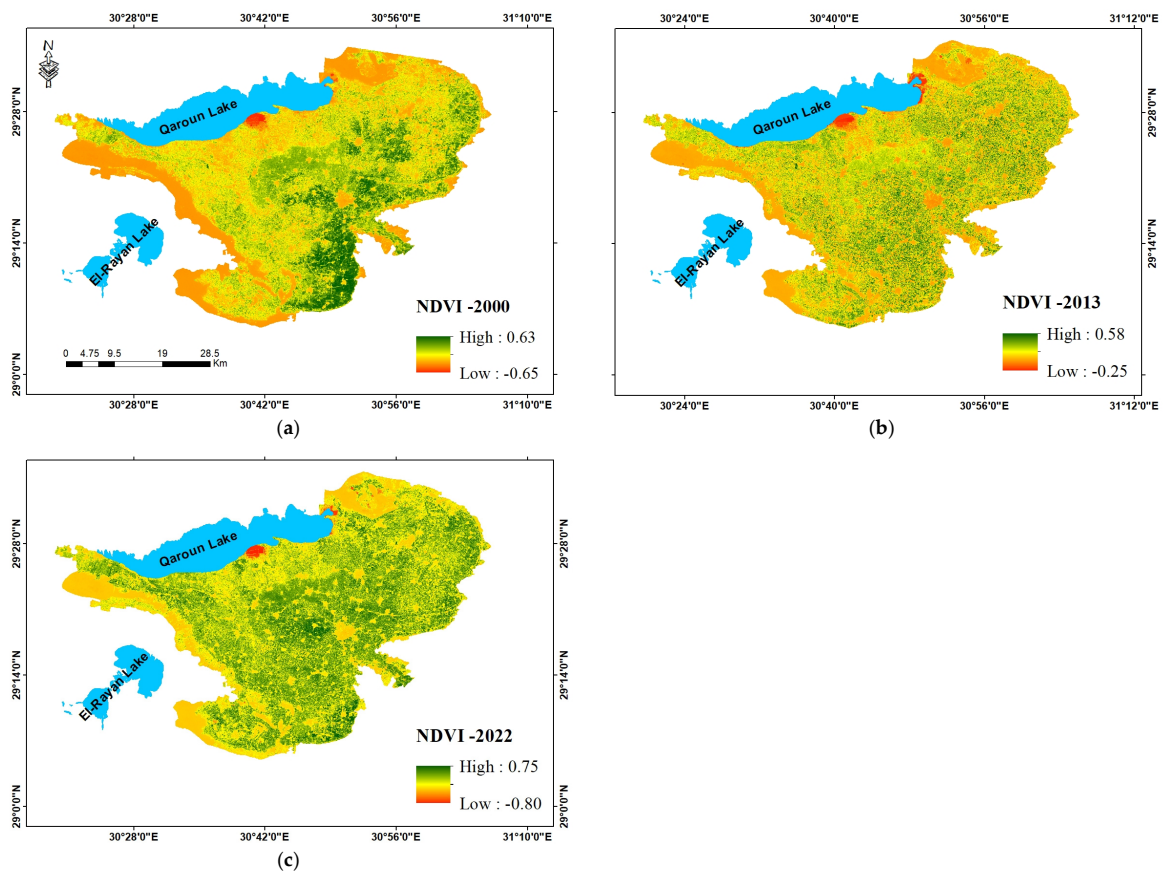


Figure 4. NDVI of study area (a) 2000, (b) 2013 and (c) 2022.

### 3.5. LST and NDVI of Study Area

The bare soil areas showed the highest mean surface temperatures, with values ranging from 41.24 °C to 43.11 °C, when LST and LULC were taken into account (Figure 5). This is consistent with the findings of [88], which similarly discovered higher LST values for exposed locations. The energy-exchange activities taking place in the soil are changed by exposing bare surfaces. In fact, soils serve as a significant heat sink, and changes to their LULC can affect the surface temperature [89]. Throughout the study period, LST values in agricultural areas ranged from about 31.87 to 41.75 °C. The mean LST values were lowest in cultivated areas because plants have the ability to selectively absorb and reflect solar radiation energy, which reduces the amount of heat absorbed in the soil by transpiration [90,91]. The maximum NDVI value in cultivated areas was 0.62, whereas the mean NDVI value on bare soil is −0.09. Consequently, bare soils are associated with lower NDVI levels (Table 5).

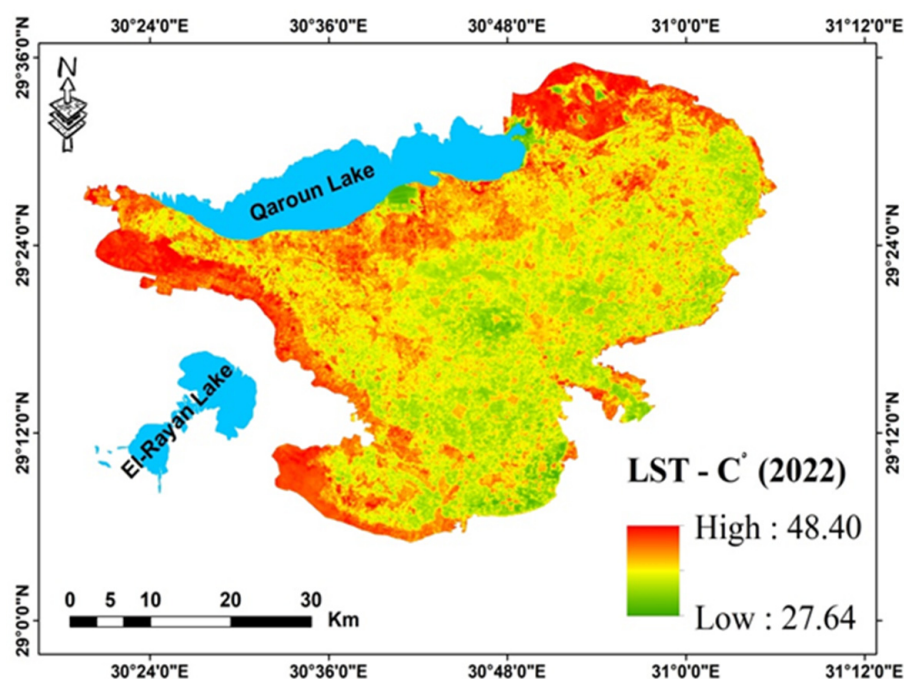


Figure 5. Land Surface Temperature (LST) of the study area.

Table 5. Statistical values of LST and NDVI in both cultivated and bare soils.

Property	N	Cultivated Areas				Bare Soils				
		Mini	Max	Mean	Std.	N	Mini	Max	Mean	Std.
LST °C	37	31.87	41.65	36.06	2.57	8	41.24	44.67	43.11	1.40
NDVI		−0.11	0.62	0.30	0.12		−0.13	−0.003	−0.09	0.044

Min. is minimum, Max is maximum and Std. is standard deviation.

### 3.6. Variation in SOCP and MEC of Study Area

The SOCP levels were quite varied, as illustrated in Figure 6a. According to variations in land use, the average concentration of SOCP in cultivated regions is 32.1 and in bare soils it is 6.5 Mg ha<sup>−1</sup>, with areas of 157,112.94 and 16,073.27 ha, respectively. Changes in soil surface, litter composition and the rate at which organic matter decomposes are the causes of possible variations in the values for organic carbon in various soils. The highest values of this attribute have been found in the agricultural region due to the possibility that an increase in carbon levels will also boost water-retention capacity [92,93]. However, the amount of organic matter in the soil affects the process of carbon mineralization and has a direct impact on the fertility and nutrient content of the soil. The rate of carbon

mineralization declines because there is less organic matter available without a constant supply of new organic matter [94]. Differences in soil textures reveal that the sandy soils have the lowest SOCP ( $1.8 \text{ Mg ha}^{-1}$ ) and the clay loam soils ( $49 \text{ Mg ha}^{-1}$ ), in agreement with [85,95], have the highest SOCP, which is falling in the east and west parts of the study area. Soil organic carbon sequestered in cultivated areas was quantified as SOCP on a larger scale. Furthermore, the regions where fruit trees are grown have the highest SOCP values and might therefore be used more successfully for carbon sequestration, which lowers overall  $\text{CO}_2$  levels and restores degraded land in these dry locations by raising soil organic carbon (SOC) contents. Fruit trees have excellent structural qualities that enable them to acquire a substantial quantity of carbon, such as a long life cycle, permanent organs like trunks, branches, and roots, zero soil tillage (maintaining soil organic matter), and high quality and yield. Consequently, fruit plants have great potential to absorb atmospheric carbon [96]. Global warming and air pollution are two challenges the globe faces today, and the two problems are interrelated. Hence, reducing air pollutant emissions while also taking steps to minimize carbon dioxide is common [97]. In terms of cropland area, the overall average SOCP values revealed  $32.12 \text{ Mg C ha}^{-1}$ . An increase in arable land led to a  $112,870.09 \text{ Mg C}$  increase in SOCP. The most important component that could be used to reduce carbon emissions from terrestrial ecosystems is farmland [98]. Carbon dioxide emissions would decrease with an increase in soil organic carbon sequestered within the soil surface. The mitigation of emitted  $\text{CO}_2$  came about as a result of expanding the cropland by  $414,233.24 \text{ Mg CO}_2$  (Figure 6b), although an increase in soil carbon storage and a decrease in soil carbon emissions can both be achieved with the right management practices, according to studies. As an illustration, consider enhancing fertilization, irrigation techniques, a multiple cropping index, lowering desertion rates, suitable crop rotation, and crop variety selection [99].

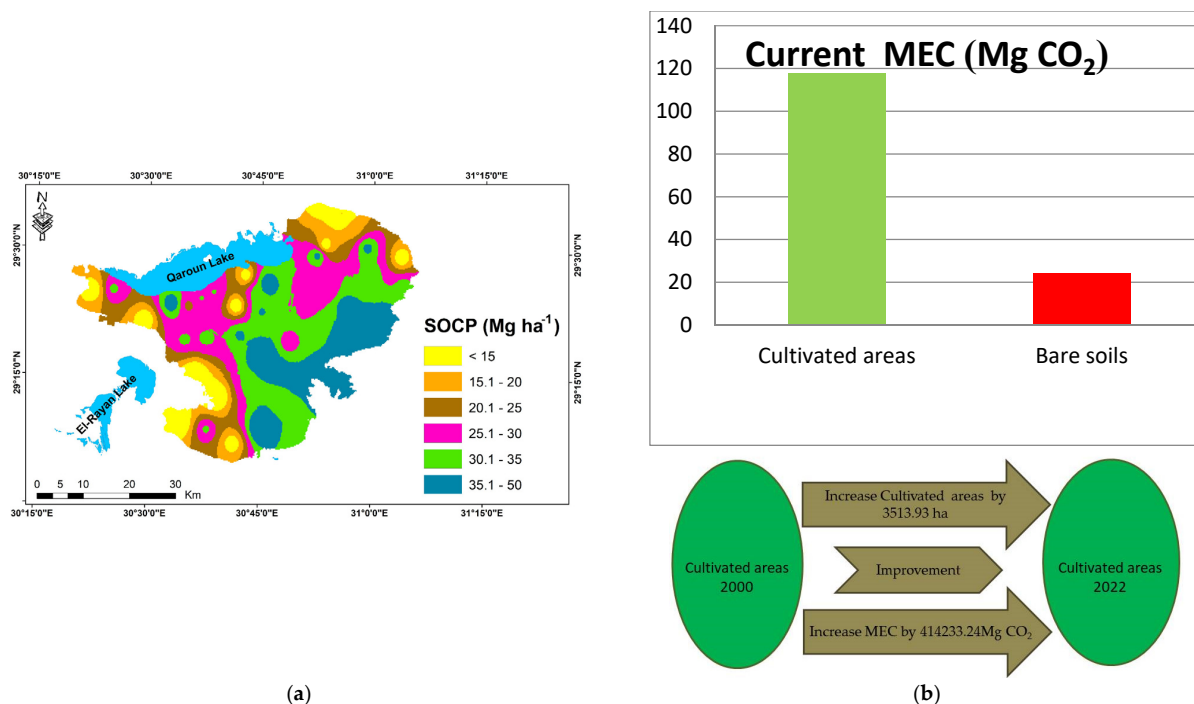


**Figure 6.** (a) The distribution of SOCP within the study area and (b) the MEC ( $\text{Mg CO}_2$ ) due to expansion of cultivated area.

#### 4. Conclusions

The main finding of this study validated our hypothesis that certain qualities, including the capacity for carbon sequestration, may be influenced by important parameters like soil texture, land use, and LST, which may then have an effect on  $\text{CO}_2$  mitigation. When

compared to soil types and different land use, the soil organic carbon pool (SOCP) in the top 30 cm of soils differed greatly. According to differences in soil texture, clay loam soils have the highest SOCP and sandy soils have the lowest SOCP. The NDVI was trustworthy indicator of the vegetation dynamics brought on by changes in land use. The NDVI and LST have a noticeable inverse relationship. If soil organic C sequestration was determined for specific soils within the various land uses on a regional scale, a higher degree of precision might be attained. Increasing the amount of arable soil through land reclamation increased the total SOCP and reduced CO<sub>2</sub> emissions, which had a favorable impact on the levels of greenhouse gases in the surrounding atmosphere. Furthermore, the areas with the greatest SOCP values could be more effectively employed for carbon sequestration, which reduces overall CO<sub>2</sub> levels and revitalizes degraded land in these arid regions by increasing soil organic carbon (SOC) contents. Fruit trees have exceptional structural characteristics that allow them to absorb a significant amount of carbon, including a long life cycle, permanent organs such trunks, branches, and roots, zero soil tillage (preserving soil organic matter), and good quality and production. The study emphasizes the value of increasing farmed land for long-term carbon sequestration and potential climate-change mitigation.

**Author Contributions:** Conceptualization, M.A.A., F.O.H., A.S.A. and M.S.S.; methodology, M.A.A., F.O.H., A.S.A. and M.S.S.; software, M.A.A., A.S.A., F.O.H. and M.S.S.; validation, M.A.A., F.O.H. and M.S.S.; formal analysis, M.A.A., F.O.H., A.S.A., S.K.A.-E. and M.S.S.; investigation, M.A.A., F.O.H., A.S.A., S.K.A.-E. and M.S.S.; resources, M.A.A., F.O.H., A.S.A. and M.S.S.; data curation, M.A.A., F.O.H. and M.S.S.; writing—original draft preparation, M.S.S.; writing—review and editing, A.A.E.B., E.S.M., H.S.A.R. and D.E.K. All authors have read and agreed to the published version of the manuscript.

**Funding:** This research received no external funding.

**Data Availability Statement:** All data are included in the manuscript.

**Acknowledgments:** This paper was supported by the RUDN University Strategic Academic Leadership Program.

**Conflicts of Interest:** The authors declare no conflict of interest.

## References

1. Lal, R. Soil Carbon Sequestration Impacts on Global Climate Change and Food Security. *Science* **2004**, *304*, 1623–1627. [[CrossRef](#)] [[PubMed](#)]
2. Manlay, R.J.; Feller, C.; Swift, M. Historical evolution of soil organic matter concepts and their relationships with the fertility and sustainability of cropping systems. *Agric. Ecosyst. Environ.* **2007**, *119*, 217–233. [[CrossRef](#)]
3. Ayoubi, S.; Karchegani, P.M.; Mosaddeghi, M.R.; Honarjoo, N. Soil aggregation and organic carbon as affected by topography and land use change in western Iran. *Soil Tillage Res.* **2012**, *121*, 18–26. [[CrossRef](#)]
4. Muñoz-Rojas, M. Modelling Carbon Sequestration Capacity in Mediterranean Soils. Ph.D. Thesis, University of Seville, Seville, Spain, 2012; p. 169.
5. Zomer, R.J.; Bossio, D.A.; Sommer, R.; Verchot, L.V. Global Sequestration Potential of Increased Organic Carbon in Cropland Soils. *Sci. Rep.* **2017**, *7*, 15554. [[CrossRef](#)]
6. Tao, F.; Palosuo, T.; Lehtonen, A.; Heikkinen, J.; Mäkipää, R. Soil organic carbon sequestration potential for croplands in Finland over 2021–2040 under the interactive impacts of climate change and agricultural management. *Agric. Syst.* **2023**, *209*, 103671. [[CrossRef](#)]
7. Bauer, A.; Black, A.L. Quantification of the Effect of Soil Organic Matter Content on Soil Productivity. *Soil Sci. Soc. Am. J.* **1994**, *58*, 185–193. [[CrossRef](#)]
8. Loveland, P. Is There a Critical Level of Organic Matter in the Agricultural Soils of Temperate Regions: A Review? *Soil Tillage Res.* **2003**, *70*, 1–18. [[CrossRef](#)]
9. Koiter, A.J.; Owens, P.N.; Petticrew, E.L.; Lobb, D.A. The Role of Soil Surface Properties on the Particle Size and Carbon Selectivity of Interrill Erosion in Agricultural Landscapes. *Catena* **2017**, *153*, 194–206. [[CrossRef](#)]
10. Cheraghi, M.; Jomaa, S.; Sander, G.C.; Barry, D.A. Hysteretic Sediment Fluxes in Rainfall-Driven Soil Erosion: Particle Size Effects. *Water Resour. Res.* **2016**, *52*, 8613–8629. [[CrossRef](#)]
11. Asadi, H.; Ghadiri, H.; Rose, C.W.; Rouhipour, H. Interrill Soil Erosion Processes and Their Interaction on Low Slopes. *Earth Surf. Process. Landf.* **2009**, *32*, 711–724. [[CrossRef](#)]

12. Wang, X.; Cammeraat, E.L.H.; Romeijn, P.; Kalbitz, K. Soil Organic Carbon Redistribution by Water Erosion—The Role of CO<sub>2</sub> Emissions for the Carbon Budget. *PLoS ONE* **2014**, *9*, e96299.
13. Wiesmeier, M.; Hübner, R.; Spörlein, P.; Geuß, U.; Hangen, E.; Reischl, A.; Schilling, B.; von Lützow, M.; Kögel-Knabner, I. Carbon Sequestration Potential of Soils in Southeast Germany Derived from Stable Soil Organic Carbon Saturation. *Glob. Chang. Biol.* **2014**, *20*, 653–665. [[CrossRef](#)]
14. Zhang, Y.; Guo, L.; Chen, Y.; Shi, T.; Luo, M.; Ju, Q.; Zhang, H.; Wang, S. Prediction of Soil Organic Carbon based on Landsat 8 Monthly NDVI Data for the Jiangnan Plain in Hubei Province, China. *Remote Sens.* **2019**, *11*, 1683. [[CrossRef](#)]
15. Rasmy, M.; Gad, A.; Abdelsalam, H.; Siwailam, M. A dynamic simulation model of desertification in Egypt. *Egypt. J. Remote Sens. Space Sci.* **2010**, *13*, 101–111. [[CrossRef](#)]
16. Johnson, J.M.F.; Franzluebbers, A.J.; Weyers, S.L.; Reicosky, D.C. Agricultural opportunities to mitigate greenhouse gas emissions. *Environ. Pollut.* **2007**, *150*, 107–124. [[PubMed](#)]
17. Snyder, C.; Bruulsema, T.; Jensen, T.; Fixen, P. Review of greenhouse gas emissions from crop production systems and fertilizer management effects. *Agric. Ecosyst.* **2009**, *133*, 247–266. [[CrossRef](#)]
18. D'Hose, T.; Coughnon, M.; De Vlieghe, A.; Vandecasteele, B.; Viaene, N.; Cornelis, W.; Van Bockstaele, E.; Reheul, D. The positive relationship between soil quality and crop production: A case study on the effect of farm compost application. *Appl. Soil Ecol.* **2014**, *75*, 189–198. [[CrossRef](#)]
19. Kačergius, A.; Sivojienė, D.; Gudiukaitė, R.; Bakšienė, E.; Masevičienė, A.; Žičkienė, L. Comparison of the Structure of Soil Microbial Communities of Different Ecosystems Using the Microbiome Sequencing Approach. *Soil Syst.* **2023**, *7*, 70. [[CrossRef](#)]
20. Chehab, H.; Tekaya, M.; Ouhibi, M.; Gouiaa, M.; Zakhama, H.; Mahjoub, Z.; Laamari, S.; Sfina, H.; Chihaoui, B.; Boujnah, D.; et al. Effects of compost, olive mill wastewater and legume cover crop on soil characteristics, tree performance and oil quality of olive trees cv. *Chemlali grown under organic farming system*. *Sci. Hortic.* **2019**, *253*, 163–171.
21. Hobley, E.U.; Baldock, J.; Wilson, B. Environmental and human influences on organic carbon fractions down the soil profile. *Agric. Ecosyst. Environ.* **2016**, *223*, 152–166. [[CrossRef](#)]
22. Assunção, S.A.; Pereira, M.G.; Rosset, J.S.; Berbara, R.L.L.; García, A.C. Carbon input and the structural quality of soil organic matter as a function of agricultural management in a tropical climate region of Brazil. *Sci. Total Environ.* **2019**, *658*, 901–911. [[CrossRef](#)] [[PubMed](#)]
23. Lal, R.; Negassa, W.; Lorenz, K. Carbon sequestration in soil. *Curr. Opin. Environ. Sustain.* **2015**, *15*, 79–86.
24. Luo, Z.; Feng, W.; Luo, Y.; Baldock, J.; Wang, E. Soil organic carbon dynamics jointly controlled by climate, carbon inputs, soil properties and soil carbon fractions. *Glob. Chang. Biol.* **2017**, *23*, 4430–4439. [[CrossRef](#)]
25. Mugwe, J.; Ngetich, F.; Otieno, E.O. Integrated Soil Fertility Management in sub-Saharan Africa Evolving Paradigms toward Integration. In *Zero Hunger. Encyclopedia of the UN Sustainable Development Goals*; Leal Filho, W., Azul, A.M., Brandli, L., Özuyar, P.G., Wall, T., Eds.; Springer International Publishing: Cham, Switzerland, 2016.
26. Hobley, E.; Wilson, B.; Wilkie, A.; Gray, J.; Koen, T. Drivers of soil organic carbon storage and vertical distribution in Eastern Australia. *Plant Soil* **2015**, *390*, 111–127.
27. Hamed, M.M.; Nashwan, M.S.; Shahid, S. Climatic zonation of Egypt based on high-resolution dataset using image clustering technique. *Prog. Earth Planet. Sci.* **2022**, *9*, 35.
28. Amantai, N.; Ding, J. Analysis on the Spatio-Temporal Changes of LST and Its Influencing Factors Based on VIC Model in the Arid Region from 1960 to 2017: An Example of the Ebinur Lake Watershed, Xinjiang, China. *Remote Sens.* **2021**, *13*, 4867. [[CrossRef](#)]
29. Li, Z.L.; Tang, B.H.; Wu, H.; Ren, H.; Yan, G.; Wan, Z.; Trigo, I.F.; Sobrino, J.A. Satellite-derived land surface temperature: Current status and perspectives. *Remote Sens. Environ.* **2013**, *131*, 14–37.
30. Owen, T.W.; Carlson, T.N.; Gillies, R.R. Remotely sensed surface parameters governing urban climate change. *Intern. J. Remote Sens.* **1998**, *19*, 1663–1681. [[CrossRef](#)]
31. Li, R.; Wang, C.; Wu, D. Changes in precipitation recycling over arid regions in the Northern Hemisphere. *Theor. Appl. Clim.* **2018**, *131*, 489–502.
32. Ali, M.G.; Ahmed, M.; Ibrahim, M.M.; El Baroudy, A.A.; Ali, E.F.; Shokr, M.S.; Aldosari, A.A.; Majrashi, A.; Kheir, A.M. Optimizing sowing window, cultivar choice, and plant density to boost maize yield under RCP8.5 climate scenario of CMIP5. *Int. J. Biometeorol.* **2022**, *66*, 971–985.
33. Yang, Y.-Y.; Goldsmith, A.; Herold, I.; Lecha, S.; Toor, G.S. Assessing Soil Organic Carbon in Soils to Enhance and Track Future Carbon Stocks. *Agronomy* **2020**, *10*, 1139. [[CrossRef](#)]
34. Lu, F.; Zhao, Y.; Huang, B.; Wang, J. Comparison of predicting methods for mapping the spatial distribution of topsoil organic matter content in cropland of hailun. *J. Soil Sci.* **2012**, *43*, 662–667.
35. Xu, E.; Zhang, H. Multi-scale analysis of kriging interpolation and conditional simulation for soil organic matters in newly reclaimed area in Yili. *Soils* **2013**, *45*, 91–98.
36. Zhao, D.; Zhao, H.; Rao, J.; Gao, X. Analysis of the spatial distribution pattern of cultivated land quality and the influential factors based on trend-surface. *Res. Soil Water Conserv.* **2015**, *22*, 219–223.
37. Zhen, J.; Pei, T.; Xie, S. Kriging methods with auxiliary nighttime lights data to detect potentially toxic metals concentrations in soil. *Sci. Total Environ.* **2019**, *659*, 363–371.

38. Abuzaid, A.S.; Mazrou, Y.S.A.; El Baroudy, A.A.; Ding, Z.; Shokr, M.S. Multi-Indicator and Geospatial Based Approaches for Assessing Variation of Land Quality in Arid Agroecosystems. *Sustainability* **2022**, *14*, 5840. [CrossRef]
39. Staff, S.S. *Keys to Soil Taxonomy*, 12th ed.; USDA-Natural Resources Conservation Service: Washington, DC, USA, 2014.
40. Abd-Elmabod, S.K.; Bakr, N.; Muñoz-Rojas, M.; Pereira, P.; Zhang, Z.; Cerdà, A.; Jordán, A.; Mansour, H.; De la Rosa, D.; Jones, L. Assessment of Soil Suitability for Improvement of Soil Factors and Agricultural Management. *Sustainability* **2019**, *11*, 1588. [CrossRef]
41. Ali, R.; Kawy, W.A. Land degradation risk assessment of El Fayoum depression, Egypt. *Arab. J. Geosci.* **2013**, *6*, 2767–2776.
42. Shokr, M.S.; Abdellatif, M.A.; El Baroudy, A.A.; Elnashar, A.; Ali, E.F.; Belal, A.A.; Attia, W.; Ahmed, M.; Aldosari, A.A.; Szantoi, Z.; et al. Development of A Spatial Model for Soil Quality Assessment under Arid and Semi-Arid Conditions. *Sustainability* **2021**, *13*, 2893. [CrossRef]
43. Abdel-Fattah, M.K.; Mohamed, E.S.; Wagdi, E.M.; Shahin, S.A.; Aldosari, A.A.; Lasaponara, R.; Alnaimy, M.A. Quantitative Evaluation of Soil Quality Using Principal Component Analysis: The Case Study of El-Fayoum Depression Egypt. *Sustainability* **2021**, *13*, 1824. [CrossRef]
44. CAPMAS. Egypt Statistical Yearbook Population. 2015. Available online: [http://www.capmas.gov.eg/Pages/Publications.aspx?page\\_id=5104&YearID=23011](http://www.capmas.gov.eg/Pages/Publications.aspx?page_id=5104&YearID=23011) (accessed on 12 July 2017).
45. Richards, L.A. *Diagnosis and Improvement of Saline and Alkali Soils*; U.S. Department of Agriculture: Washington, DC, USA, 1954; Volume 78, p. 154.
46. Van Reeuwijk, L.P. Procedures for Soil Analysis. *Tech. Pap.-Int. Soil Ref. Inf. Cent.* **1986**, *9*, 106. Available online: <https://pascal-francis.inist.fr/vibad/index.php?action=getRecordDetail&idt=8009739> (accessed on 3 February 2021).
47. USDA. Soil Survey Laboratory Methods Manual. *Soil Surv. Investig. Rep.* **2004**, *42*, 31–247.
48. Baruah, T.; Barthakur, H. *A Textbook of Soil Analysis*; Vikas Publishing House PVT Ltd.: New Delhi, India, 1997.
49. Kettler, T.A.; Doran, J.W.; Gilbert, T.L. Simplified method for soil particle-size determination to accompany soil-quality analyses. *Soil Sci. Soc. Am. J.* **2001**, *65*, 849–852.
50. Bogunovic, I.; Kljak, K.; Dugan, I.; Grbeša, D.; Telak, L.J.; Duvnjak, M.; Kisić, I.; Solomun, M.K.; Pereira, P. Grassland Management Impact on Soil Degradation and Herbage Nutritional Value in a Temperate Humid Environment. *Agriculture* **2022**, *12*, 921. [CrossRef]
51. Ahogle, A.M.A.; Alladassi, F.K.; Akplo, T.M.; Azontonde, H.A.; Houngnandan, P. Assessing Soil Organic Carbon Stocks and Particle-Size Fractions across Cropping Systems in the Kiti Sub-Watershed in Central Benin. *C* **2022**, *8*, 67. [CrossRef]
52. Abdelsamie, E.A.; Abdellatif, M.A.; Hassan, F.O.; El Baroudy, A.A.; Mohamed, E.S.; Kucher, D.E.; Shokr, M.S. Integration of RUSLE Model, Remote Sensing and GIS Techniques for Assessing Soil Erosion Hazards in Arid Zones. *Agriculture* **2023**, *13*, 35. [CrossRef]
53. Isaaks, E.H.; Srivastava, M.R. *Applied Geostatistics*; Oxford University Press: New York, NY, USA, 1989.
54. Johnston, K.; Ver Hoef, J.M.; Krivoruchko, K.; Lucas, N. *Using ArcGIS Geostatistical Analyst*; ESRI: Redlands, CA, USA, 2001; Volume 380.
55. Gundogdu, K.S.; Guney, I. Spatial analyses of groundwater levels using universal kriging. *J. Earth Syst. Sci.* **2007**, *116*, 49–55. [CrossRef]
56. Abdellatif, M.A.; El Baroudy, A.A.; Arshad, M.; Mahmoud, E.K.; Saleh, A.M.; Moghanm, F.S.; Shaltout, K.H.; Eid, E.M.; Shokr, M.S. A GIS-Based Approach for the Quantitative Assessment of Soil Quality and Sustainable Agriculture. *Sustainability* **2021**, *13*, 13438. [CrossRef]
57. Mohamed, E.S.; Jalhoum, M.E.M.; Belal, A.A.; Hendawy, E.; Azab, Y.F.A.; Kucher, D.E.; Shokr, M.S.; El Behairy, R.A.; El Arwash, H.M. A Novel Approach for Predicting Heavy Metal Contamination Based on Adaptive Neuro-Fuzzy Inference System and GIS in an Arid Ecosystem. *Agronomy* **2023**, *13*, 1873. [CrossRef]
58. Abuzaid, A.S.; Jahin, H.S.; Shokr, M.S.; El Baroudy, A.A.; Mohamed, E.S.; Rebouh, N.Y.; Bassouny, M.A. A Novel Regional-Scale Assessment of Soil Metal Pollution in Arid Agroecosystems. *Agronomy* **2023**, *13*, 161. [CrossRef]
59. Lillesand, T.M.; Kiefer, R.W. *Remote Sensing and Image Interpretation*; Wiley: Hoboken, NJ, USA, 2000.
60. U.S. Geological Survey. Landsat Missions: Using the USGS Landsat Level-1 Data Product. 2021. Available online: <https://www.usgs.gov/landsat-missions/using-usgs-landsat-level-1-data-product> (accessed on 1 October 2022).
61. Avdan, U.; Jovanovska, J. Algorithm for Automated Mapping of Land Surface Temperature Using LANDSAT 8 Satellite Data. *J. Sens.* **2016**, *2016*, 1480307. [CrossRef]
62. Aman, A.; Randriamanantena, H.P.; Podaire, A.; FROUTIN, R. Upscale Integration of Normalized Difference Vegetation Index: The Problem of Spatial Heterogeneity. *IEEE Trans. Geosci. Remote Sens.* **1992**, *30*, 326–338. [CrossRef]
63. Rouse Jr, J.W.; Haas, R.H.; Deering, D.W.; Schell, J.A.; Harlan, J.C. *Monitoring the Vernal Advancement and Retrogradation (Green Wave Effect) of Natural Vegetation*; No. E75-10354; NTRS: Washington, DC, USA, 1974.
64. Barsi, J.A.; Schott, J.R.; Hook, S.J.; Raqueno, N.G.; Markham, B.L.; Radocinski, R.G. Landsat-8 Thermal Infrared Sensor (TIRS) Vicarious Radiometric Calibration. *Remote Sens.* **2014**, *6*, 11607–11626. [CrossRef]
65. Tan, Z.X.; Lal, R. Carbon sequestration potential estimates with changes in land use and tillage practice in Ohio, USA. *Agric. Ecosyst. Environ.* **2005**, *111*, 140–152.
66. Intergovernmental Panel on Climate Change—IPCC. *Fourth Assessment Report; Climate Change Synthesis Report*; Cambridge University Press: Cambridge, UK, 2007.

67. Curtin, D.; Campbell, C.; Jalil, A. Effects of acidity on mineralization: pH-dependence of organic matter mineralization in weakly acidic soils. *Soil Biol. Biochem.* **1998**, *30*, 57–64.
68. FAO; United Nations Environment Programme; United Nations Educational, Scientific, and Cultural Organization. *A Provisional Methodology for Soil Degradation Assessment*; FAO: Rome, Italy, 1980.
69. El Behairy, R.A.; El Baroudy, A.A.; Ibrahim, M.M.; Kheir, A.M.; Shokr, M.S. Modelling and assessment of irrigation water quality index using GIS in semi-arid region for sustainable agriculture. *Water Air Soil Pollut.* **2021**, *232*, 352.
70. Zhenghu, D.; Honglang, X. Effects of soil properties on ammonia volatilization. *Soil Sci. Plant Nutr.* **2000**, *46*, 845–852.
71. Wandruszka, R.V. Phosphorus retention in calcareous soils and the effect of organic matter on its mobility. *Geochem. Trans.* **2006**, *7*, 6.
72. Obalum, S.E.; Chibuike, G.U.; Peth, S.; Ouyang, Y. Soil organic matter as sole indicator of soil degradation. *Environ. Monit. Assess.* **2017**, *189*, 176. [[CrossRef](#)] [[PubMed](#)]
73. Wang, D.-C.; Zhang, G.-L.; Zhao, M.-S.; Pan, X.-Z.; Zhao, Y.-G.; Li, D.-C.; Macmillan, B. Retrieval and Mapping of Soil Texture Based on Land Surface Diurnal Temperature Range Data from MODIS. *PLoS ONE* **2015**, *10*, e0129977. [[CrossRef](#)]
74. Leifeld, J.; Bassin, S.; Fuhrer, J. Carbon stocks in Swiss agricultural soils predicted by land-use, soil characteristics, and altitude. *Agric. Ecosyst. Environ.* **2005**, *105*, 255–266.
75. Tanveera, A.; Kanth, T.A.; Tali, P.A.; Naikoo, M. Relation of Soil Bulk Density with Texture, Total Organic Matter Content and Porosity in the Soils of Kandi Area of Kashmir Valley, India. *Int. Res. J. Earth Sci.* **2016**, *4*, 1–6.
76. Miles, N.; Meyer, J.H.; Van Antwerpen, R. Soil organic matter data: What do they mean. *Proc. S. Afr. Sugar Technol. Assoc.* **2008**, *81*, 324–332.
77. Russel, E.J. *Soil Conditions and Plant Growth*, 10th ed.; Longman: London, UK, 1973.
78. Bresler, E.; Dagan, G.; Wagenet, R.J.; Laufer, A. Statistical analysis of salinity and texture effects on spatial variability of soil hydraulic conductivity. *Soil Sci. Soc. Am. J.* **1984**, *48*, 16–25.
79. Frenkel, H.; Goertzen, J.O.; Rhoades, J.D. Effects of clay type and content, exchangeable sodium percentage, and electrolyte concentration on clay dispersion and soil hydraulic conductivity. *Soil Sci. Soc. Am. J.* **1978**, *42*, 32–39.
80. Wang, S.; Zhuang, Q.L.; Wang, Q.B.; Jin, X.X.; Han, C.L. Mapping stocks of soil organic carbon and soil total nitrogen in liaoning province of china. *Geoderma* **2017**, *305*, 250–263.
81. Kumar, K.S.; Bhaskar, P.U.; Padmakumari, K. Estimation of land surface temperature to study urban heat island effect using Landsat ETM+ image. *Int. J. Eng. Sci. Technol.* **2012**, *4*, 771–778.
82. Ullah, S.; Tahir, A.A.; Akbar, T.A.; Hassan, Q.K.; Dewan, A.; Khan, A.J.; Khan, M. Remote Sensing-Based Quantification of the Relationships between Land Use Land Cover Changes and Surface Temperature over the Lower Himalayan Region. *Sustainability* **2019**, *11*, 5492. [[CrossRef](#)]
83. Hassan, F.O. Assessment of Soil and Water Quality and Their Effect on Agriculture Productivity in El-Fayoum Governorate, Egypt Using Remote Sensing and GIS Techniques. Ph.D. Thesis, Soil and Water Department, Faculty of Agriculture, Benha University, Banha, Egypt, 2022.
84. El-Nady, M.F.; El-Hady, O.A.; El-Sebaie, O.A. Land evaluation for planting some fruit trees in Fayoum Governorate, Egypt. *Land Degrad. Dev.* **2015**, *26*, 431–441. [[CrossRef](#)]
85. Abou-Seeda, M.A.; Khalafallah, M.G.; Bayoumi, A.T. A combined approach for evaluating land suitability for wheat in the Fayoum Oasis, Egypt. *J. Soil Sci. Agric. Eng.* **2013**, *4*, 527–541.
86. Abu-hashim, M.; Elsayed, M.; Belal, A.E. Effect of land-use changes and site variables on surface soil organic carbon pool at Mediterranean Region. *J. Afr. Earth Sci.* **2016**, *114*, 78–84.
87. Muster, S.; Langer, M.; Abnizova, A.; Young, K.L.; Boike, J. Spatio-temporal sensitivity of MODIS land surface temperature anomalies indicates high potential for large-scale land cover change detection in Arctic permafrost landscapes. *Remote Sens. Environ.* **2015**, *168*, 1–12.
88. Onwuka, B.; Mang, B. Effects of soil temperature on some soil properties and plant growth. *Adv. Plants Agric Res.* **2018**, *8*, 34–37.
89. Hillel, D. *Introduction to Environmental Soil Physics*; Elsevier Academic 637 Press: Amsterdam, The Netherlands, 2004; p. 494.
90. Yuan, X.L.; Wang, W.; Cui, J.; Meng, F.; Kurban, A.; Maeyer, P. Vegetation changes and land surface feedbacks drive shifts in local temperatures over Central Asia. *Sci. Rep.* **2017**, *7*, 3287.
91. Xin, Z.; Qin, Y.; Yu, X. Spatial Variability in Soil Organic Carbon and Its Influencing Factors in a Hilly Watershed of the Loess Plateau, China. *Catena* **2016**, *137*, 660–669.
92. Chiriluş, G.V.; Lakatos, E.S.; Bălc, R.; Bădărău, A.S.; Cioca, L.I.; David, G.M.; Roşian, G. Assessment of Organic Carbon Sequestration from Romanian Degraded Soils: Livada Forest Plantation Case Study. *Atmosphere* **2022**, *13*, 1452. [[CrossRef](#)]
93. Rawls, W.J.; Pachepsky, Y.A.; Ritchie, J.C.; Sobecki, T.M.; Bloodworth, H. Effect of Soil Organic Carbon on Soil Water Retention. *Geoderma* **2003**, *116*, 61–76.
94. Korkanç, S.Y. Effects of Afforestation on Soil Organic Carbon and Other Soil Properties. *Catena* **2014**, *123*, 62–69.
95. Lantz, A.M.; Lal, R.; Kimble, J.M. Land-use effects on soil carbon pools in three major land resource areas of Ohio. In *Agricultural Practices and Policies for Carbon Sequestration in Soil*; Kimble, J.M., Lal, R., Follett, R., Eds.; Lewis Publishers: Boca Raton, FL, USA, 2002; pp. 165–175.
96. Sharma, S.; Rana, V.S.; Prasad, H.; Lakra, J.; Sharma, U. Appraisal of carbon capture, storage, and utilization through fruit crops. *Front. Environ. Sci.* **2021**, *9*, 700768.

97. Xie, X.; Weng, Y.; Cai, W. Co-Benefits of CO<sub>2</sub> Mitigation for NO<sub>x</sub> Emission Reduction: A Research Based on the DICE Model. *Sustainability* **2018**, *10*, 1109. [[CrossRef](#)]
98. Zhu, G.; Qiu, D.; Zhang, Z.; Sang, L.; Liu, Y.; Wang, L.; Zhao, K.; Ma, H.; Xu, Y.; Wan, Q. Land-use changes lead to a decrease in carbon storage in arid region, China. *Ecol. Indic.* **2021**, *127*, 107770.
99. Chen, G.; Tian, H. Land Use/Cover Change Effects on Carbon Cycling in Terrestrial Ecosystems. *Chin. J. Plant Ecol.* **2007**, *31*, 189–204. (In Chinese) [[CrossRef](#)]

**Disclaimer/Publisher's Note:** The statements, opinions and data contained in all publications are solely those of the individual author(s) and contributor(s) and not of MDPI and/or the editor(s). MDPI and/or the editor(s) disclaim responsibility for any injury to people or property resulting from any ideas, methods, instructions or products referred to in the content.